

## REFERENCES

1. LLE Review **33**, 1 (1988).
2. Y. Kato *et al.*, Phys. Rev. Lett. **53**, 1057 (1984).
3. L. B. Lesem, P. M. Hirsch, and J. A. Jordan, Jr., IBM J. Res. Develop. **13**, 150 (1969).
4. X. Deng *et al.*, Appl. Opt. **25**, 377 (1986).
5. P. Langois and R. Beaulieu, Appl. Opt. **29**, 3434 (1990).
6. T. Jitsuno *et al.*, presented at CLEO '92, paper CThI2.
7. H. Dammann and K. Görtler, Opt. Commun. **3**, 312 (1971).
8. J. Jahns *et al.*, Opt. Eng. **28**, 1267 (1989).
9. U. Krackhardt, J. N. Mait, and N. Streibl, Appl. Opt. **31**, 27 (1992).
10. N. Streibl, J. Mod. Opt. **36**, 1559 (1989).
11. D. Daly, S. M. Hodson, and M. C. Hutley, Opt. Commun. **82**, 183 (1991).
12. P. Ehbets *et al.*, Opt. Lett. **17**, 908 (1992).
13. D. Prongué *et al.*, Appl. Opt. **31**, 5706 (1992).
14. R. W. Gerchberg and W. O. Saxton, OPTIK **35**, 237 (1972).
15. J. R. Fienup, Appl. Opt. **21**, 2758 (1982).
16. K. Ichikawa, A. W. Lohmann, and M. Takeda, Appl. Opt. **27**, 3433 (1988).
17. P. E. Keller and A. F. Gmitro, submitted to Applied Optics.

## 2.B Nematic Polymer Liquid-Crystal Wave Plate for High-Power Lasers at 1054 nm

Liquid-crystalline materials capable of replacing traditional crystalline solids in the production of wave plates are becoming more desirable due to the high cost of the solid crystals typically used,<sup>1</sup> including natural and synthetic mica, quartz, sapphire, magnesium fluoride, and KDP (potassium dihydrogen phosphate). The laborious and often expensive process of high-precision optical polishing of plates fabricated from these crystals makes their use still less feasible for large-aperture requirements. In addition, the range of available retardance values is limited, and the laser-damage thresholds are not always known.<sup>1</sup>

Low-molecular-weight liquid-crystal monomers (LMLC's) have overcome the cost disadvantages of typical solid crystals. LMLC's are particularly successful in meeting specific retardance needs and can exhibit high resistance to pulsed-laser damage in IR and UV regimes.<sup>2</sup> Despite their many successes, LMLC's introduce some difficulties of their own—the use of thick glass substrates to support the LC without bowing and the epoxy sealing of these substrates without long-term transmitted-wavefront distortion due to the sealant.<sup>3</sup>

Polymer liquid crystals (PLC's) potentially meet the same needs as monomeric LMLC's but without their difficulties. PLC's generally have a high isotropic transition temperature. At and above this temperature, PLC's can be manipulated like LMLC's. At lower temperatures, the polymers become viscous enough to maintain their chosen configuration. The polymer also acts as its own substrate sealant, eliminating the need for epoxies.<sup>4</sup>

Here, we examine the properties of a nematic PLC (NPLC) aligned using a buffed nylon<sup>5</sup> 6/6 layer. Properties studied include viscosity (temperature dependence), birefringence (dispersion and temperature dependence), and laser-damage resistance. We describe three techniques to construct NPLC wave plates and evaluate the uniformity and transmitted wavefront quality of several 50-mm-diam devices.

### Properties of Nematic Polymer Liquid Crystal

#### 1. Structure and Physical Properties

The liquid-crystal polymer used for this study, LC360N, is a side-chain polymer with polysiloxane backbone<sup>6</sup> (see Fig. 55.25). The polymer's glass transition temperature and clearing temperature are 23°C and 88°C, respectively. Its viscosity at room temperature (22°C) is greater than  $3 \times 10^8$  cp ( $3 \times 10^5$  Pa-s), making it sticky to the touch. Since its dielectric anisotropy is nearly zero, it does not afford alignment by application of an electric field.

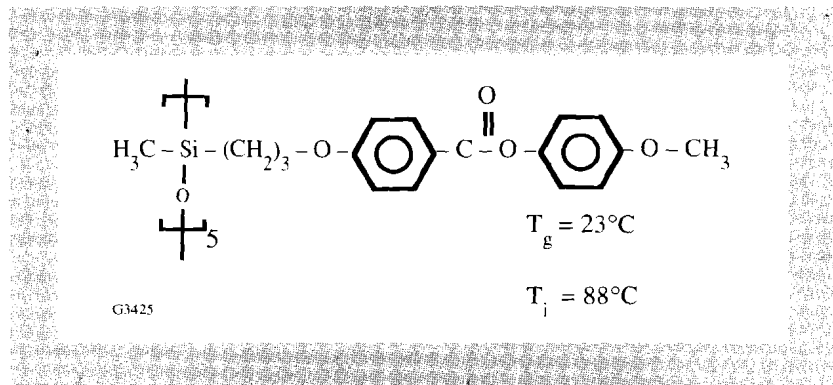


Fig. 55.25

Structure of the NPLC LC360N. The polysiloxane backbone is shown on the left.

#### 2. Viscosity

For a PLC to be useful in optical devices like wave plates, it must have a high viscosity at the temperature at which the device is to be used to ensure device stability. The PLC must also have a low enough viscosity at some convenient temperature to facilitate both alignment and device construction. LC360N meets both of these requirements as determined by a viscosity/temperature measurement.

Viscosity was measured using a commercial digital viscometer equipped with a helipath accessory.<sup>7</sup> The viscometer rotated a spindle and measured the force required to maintain a chosen rotational speed against the viscous drag of the sample; this force was directly related to the viscosity. The sample container had an inner diameter of 1.8 cm and the sample volume was 12 ml. For LC360N, at low temperatures ( $T < 80^\circ\text{C}$ ), a T-bar-type spindle (1.09-cm crossbar length) was used with helical path action. A stand raised and lowered the sample at a rate of 2.22 cm/min through a distance of 2.3 cm around the rotating spindle to ensure

that the spindle continuously encountered fresh polymer, i.e., not previously grooved. At high temperatures ( $T > 80^\circ\text{C}$ ), the usual disc-type spindle (1.46-cm diam) without the helipath accessory was used. As a result, there was a wider range of measured values for the higher viscosities (lower temperatures) due to the action of raising and lowering the spindle. Rotational speed was varied from 0.5 to 100 rpm. Since a different speed was optimum at each temperature, the viscosity reading was used when the digital reading was 10% of the maximum range available for the given spindle/speed combination. (Results are shown in Fig. 55.26.) The data were fitted empirically to give the relationship

$$\ln(\eta/\eta_i) = 1.03 \times 10^7 (1/T)^2 - 4.69 \times 10^4 (1/T) + 51.33 , \quad (1)$$

where  $\eta$  is the viscosity in centipoise,  $\eta_i$  is the viscosity in centipoise at the isotropic temperature, and  $T$  is the absolute temperature ( $^\circ\text{K}$ ). The temperature was maintained using a circulating-water jacket;<sup>8</sup> the water-bath temperature supplying the jacket was controllable to  $\pm 0.01^\circ\text{C}$  accuracy. Our results showed no sharp change in viscosity at the nematic/isotropic transition, as has been reported by others for lyotropic polymers<sup>9</sup> and for thermotropic LMLC's.<sup>10</sup> At the N/I transition, the apparent viscosity was  $6.78 \pm 0.25 \times 10^3 \text{ cp}$  ( $6.78 \pm 0.25 \text{ Pa-s}$ ). At room temperature ( $22^\circ\text{C}$ ), the empirical fit projects an apparent viscosity of  $3 \times 10^8 \text{ cp}$  ( $3 \times 10^5 \text{ Pa-s}$ ), comparable to taffy. These data confirm that flow and alignment can be accomplished at elevated temperatures with the alignment "frozen in" at a glass transition at or above room temperature.

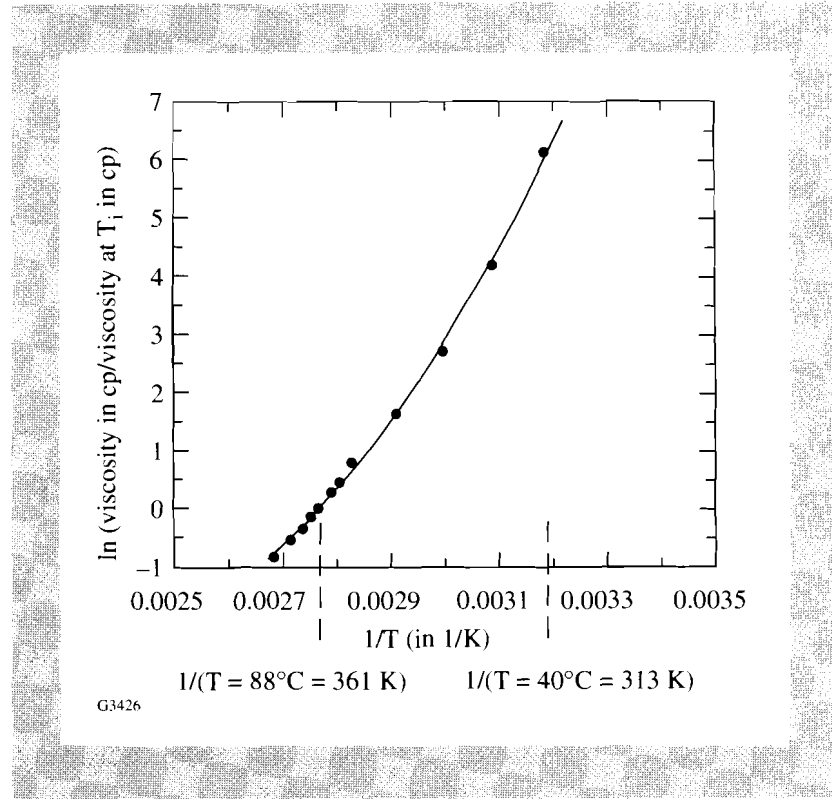


Fig. 55.26  
Temperature dependence of NPLC viscosity. Viscosity is determined as a function of temperature using a rotating-spindle-type viscometer. Measurements for temperatures below  $80^\circ\text{C}$  are made using a T-bar spindle with helical path action. Measurements for temperatures at and above  $80^\circ\text{C}$  are made using a disc-type spindle and no helical action.

### 3. Birefringence Measurement: Method and Results

The birefringence of the NPLC must be accurately known to construct a wave plate with the desired retardance. Measurements of the ordinary and extraordinary refractive indices were performed using a commercial Abbe refractometer.<sup>11</sup> The refractometer was calibrated<sup>12</sup> with a fused-silica standard at each wavelength/temperature combination used. Due to the high viscosity of LC360N at room temperature, placing it directly on the refractometer stage is inconvenient, and polymer alignment is difficult. For this side-chain polysiloxane, the side chains are responsible for the birefringence. Without an alignment layer on the substrate, the side chains align homeotropically. When a rubbed alignment layer is used, the side chains align along the rub direction.<sup>13</sup> We chose the latter configuration since alignment quality could be checked quickly by viewing between crossed polarizers. The refractive indices were determined with a cell constructed by sandwiching the NPLC between  $S_1$ , a high-index glass plate (SF4,  $n_D = 1.76$ ), and  $S_2$ , a low-index glass plate (microscope slide,  $n_D \approx 1.5$ ) [see Fig. 55.27(a) inset], both of which had been prepared with a nylon 6/6 alignment layer in the following manner:

The glass substrate surfaces intended for contacting the NPLC were covered with 88% (reagent grade) formic acid for 30 s, spun at 1900 rpm for 60 s, then covered with a 0.2% solution of nylon 6/6 in 88% formic acid for 60 s and spun at 1900 rpm for 2 min. The coated substrates were heated on a programmable hotplate<sup>14</sup> at 115°C (15°C above the boiling point of formic acid to ensure complete evaporation of the solvent) for 1½ h and allowed to cool to room temperature. The coated substrate was buffed by a device developed in-house (at LLE). It consisted of a spinning (2000 rpm) cylinder, 25 cm long and 10 cm in diameter and covered with a polyaramide fiber sheet.<sup>15</sup> The substrate was held to a platform by vacuum and then passed beneath the rotating cylinder. The height of the roller was adjusted until passing the substrate under the stationary roller just caused light behind the roller to be extinguished. The direction of buffing was defined as the direction of the roller motion (same as movement of the platform for first pass). The substrate was passed forward and backward under the spinning roller four times.

The NPLC and the SF4 plate were heated to 100°C. The NPLC was dabbed by microspatula onto the SF4 plate and covered with the unheated, low-index plate so that the rub directions of the substrates were antiparallel. No spacers were used. This cell was placed directly on a hotplate, held at 88°C ( $T_i$ ) for 24 h, and then cooled from 88°C to 20°C at a rate of 1°C/h. Using a contact micrometer,<sup>16</sup> the thickness of the NPLC layer was determined to be approximately 20 µm. The same sandwich cell was used for all birefringence measurements.

$S_1$  was mounted on the very-high-index ( $n_D = 1.92$ ) refractometer prism with a fluid whose refractive index was  $n_D = 1.81$ .<sup>17</sup> The Abbe refractometer and sample arrangement are shown in Fig. 55.27(a). Although the flatness of substrates  $S_1$  and  $S_2$  was poorer than  $4\lambda$  at 633 nm, the NPLC alignment quality was sufficient for the measurements. The index of  $S_2$  was not critical. (If the index of  $S_2$  happened to be higher than the NPLC,  $S_2$  would not couple light into the sandwich cell, and the existence of  $S_2$  would simply not register.) The cell was

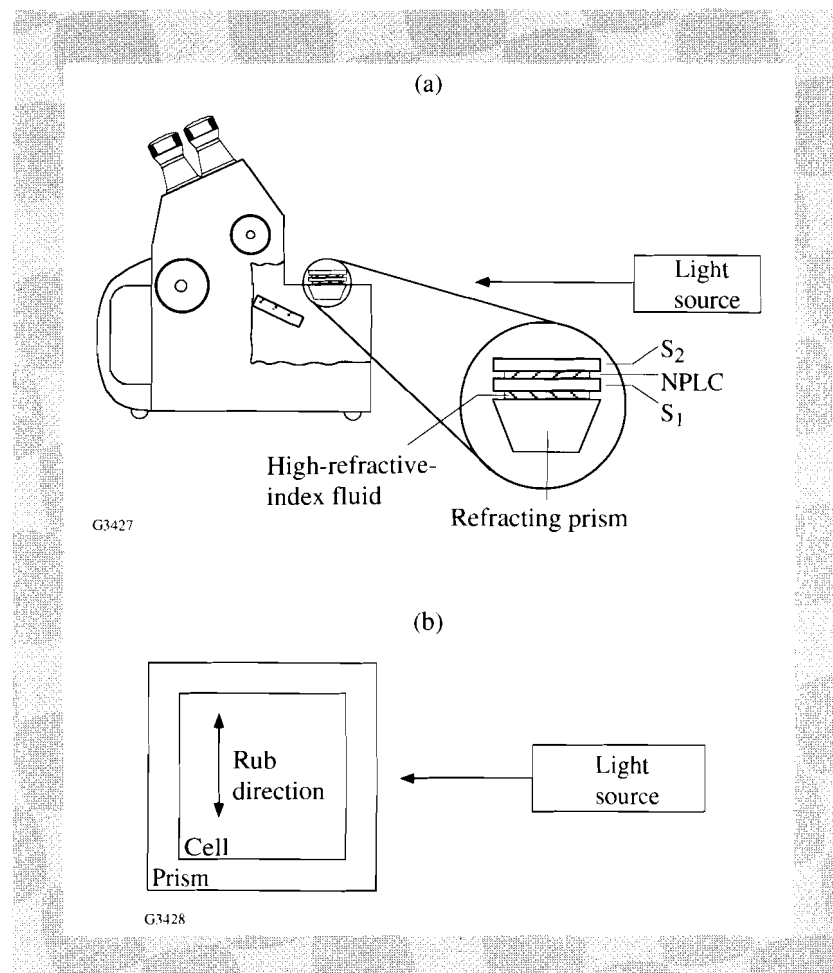


Fig. 55.27

Schematic diagram of Abbe refractometer and sample. (a) The refracting prism has the highest refractive index; index-matching fluid has a refractive index between  $S_1$  and the refracting prism;  $S_1$  is a high-index glass substrate; NPLC is the nematic polymer liquid crystal aligned by thermal annealing between substrates prepared with a rubbed polymer alignment layer;  $S_2$  is a glass substrate of arbitrary refractive index. Source light is directed through the sample onto a mirror and then to the observer. The mirror is rotated to detect the critical angle used to calculate the refractive index. (b) The sample cell is oriented on the Abbe prism with the direction of buffing orthogonal to the incoming light beam.

oriented on the refractometer stage such that the light from the source would sample both the ordinary and extraordinary indices. The rub direction was orthogonal to the incoming light beam [see Fig. 55.27(b)]. Both  $n_o$  and  $n_e$  measurements were read in this configuration; five trials of each were averaged.

The ordinary and extraordinary refractive indices were measured at 20°C for various wavelengths. The indices, their average values

$$\left\{ n_{av} = \left[ (2n_o^2 + n_e^2)/3 \right]^{1/2} \right\}$$

and the birefringence values are shown with their standard deviations,  $\sigma_{N-1}$ , in Table 55.II. The light sources used were sodium lamp, mercury lamp, HeNe laser, and Nd:YLF laser. The sodium and mercury sources were unpolarized. The polarized HeNe and Nd:YLF beams were passed through a diffuser to randomize the polarization. The Abbe refractometer makes use of the critical-angle relationship of the sample with the refractometer prism. The observer sees a split light-field, darker where the critical angle for a given sample index is exceeded. The lighter part of the field of view is illuminated by the light source. To see the split field when using an IR source, a hand-held IR scope<sup>18</sup> was held at the

Table 55.II: Refractive indices of NPLC at 20°C.

Source	Wavelength (nm)	$n_o$	$n_e$	$\Delta n$	$n_{av}$
Hg	546.1	1.5320±0.0002	1.6960±0.0004	0.1640±0.0006	1.5885±0.0003
Na	589.6	1.5269±0.00005	1.6864±0.0003	0.1595±0.00035	1.5819±0.0001
HeNe	632.8	1.5251±0.0002	1.6816±0.0003	0.1565±0.0005	1.5790±0.0002
Nd:YLF	1054	1.5132±0.0002	1.6584±0.0002	0.1452±0.0004	1.5631±0.0002

eyepiece, and measurements were then made in the usual manner. Three points ( $\lambda = 546.1, 632.8$ , and 1054 nm) were used to fit these data to the Cauchy equation:

$$n = A + B/\lambda^2 + C/\lambda^4 \quad . \quad (2)$$

The coefficients for  $n_o$  and  $n_e$  are shown in Table 55.III. The individual curves in Fig. 55.28(a) were subtracted point by point to give the birefringence dispersion curve in Fig. 55.28(b). The birefringence dispersion of crystalline quartz,<sup>19</sup> shown in Fig. 55.28(b) for comparison, is approximately 15 times smaller than that of LC360N.

The refractive indices were determined at 1054 nm for various temperatures. Temperature was maintained using a circulating-water bath<sup>8</sup> around the refracting prism. These indices are listed in Table 55.IV. The temperature dependence of the ordinary and extraordinary indices is shown in Fig. 55.29(a). The temperature dependence of the birefringence of our NPLC (LC360N) and that of several other LC's are listed in Table 55.V and plotted on Fig. 55.29(b). Other LC's shown are another NPLC (methylstilbene PLC<sup>20</sup>) but at 589.6 nm, an LMLC (K15<sup>21,22</sup>) at 1054 nm, an LLE mixture (60% 18523 and 40% 14627<sup>3,22</sup> by weight) at 1047 nm, and an LMLC (E200<sup>22</sup>) at 1047 nm.

Table 55.III: Coefficients of Cauchy equation for dispersion of ordinary and extraordinary indices of refraction for NPLC at 20°C.

	A	B	C
$n_o$	1.5071	$6.6064 \times 10^{-3}$	$2.4866 \times 10^{-8}$
$n_e$	1.6474	$1.1344 \times 10^{-4}$	$9.3661 \times 10^{-8}$

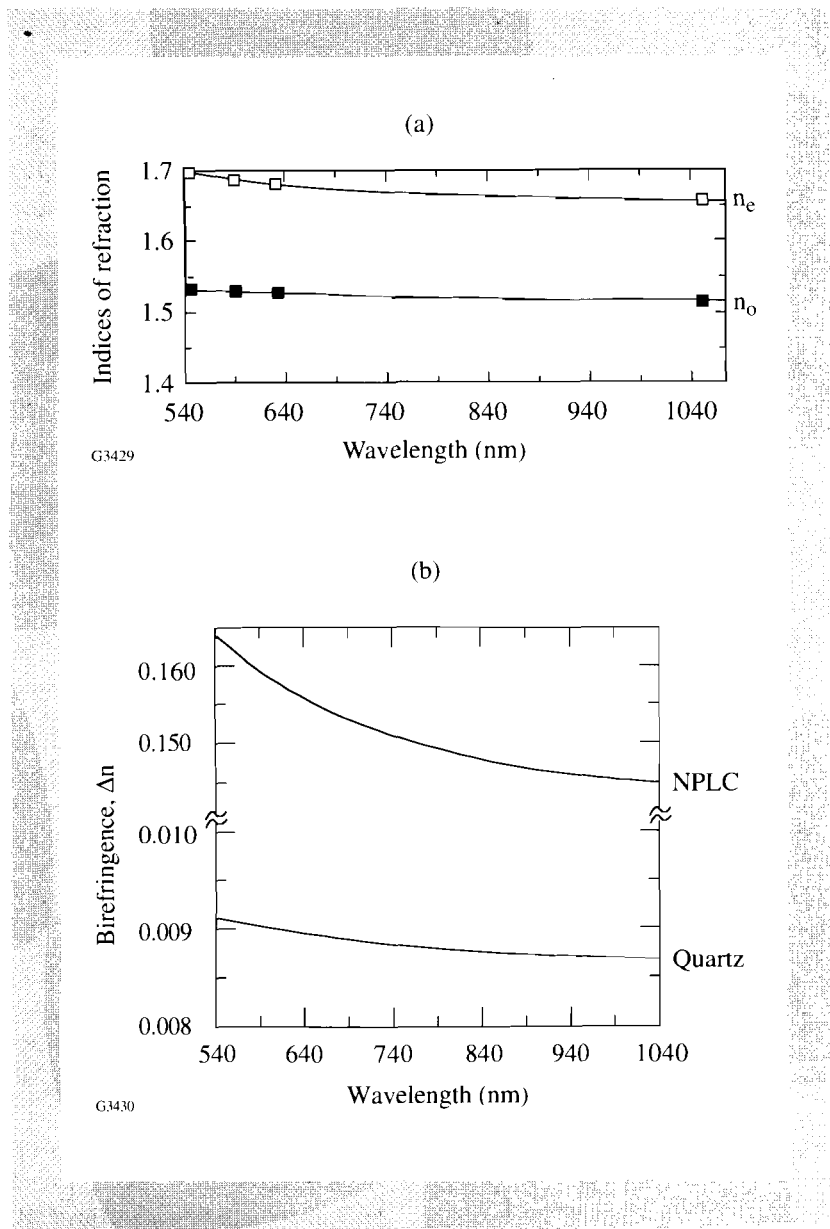


Fig. 55.28

Dispersion of refractive index of NPLC. (a) The ordinary and extraordinary refractive indices of the NPLC are fitted separately to the Cauchy equation. (b) The ordinary and extraordinary indices curves are subtracted point by point to yield the dispersion curve. All index dispersion measurements are determined at 20°C. Birefringence dispersion for crystalline quartz<sup>19</sup> is shown for the same range.

For LC360N, an empirical second-order polynomial fit of birefringence versus temperature (°C) yields a  $d(\Delta n)/dT$  at 20°C of (-)0.0003/°C. At room temperature, the birefringence change per degree is within the standard deviation of the birefringence value. A wave plate made with this NPLC would show a variation in retardance at room temperature of only 0.3 nm/°C per micron of polymer thickness. In a zero-order half-wave plate, this represents a retardance

change per °C of only 0.15 nm. By comparison, the methylstilbene polymer shows a variation in retardance of 0.03 nm/°C/μm but, due to its lower birefringence, would require a thicker cell to produce the same retardance as our NPLC. The LMLC's show a wide variation of the temperature dependence of birefringence. The LMLC K15 exhibits a very large birefringence change with temperature at 20°C. This is to be expected since its clearing temperature is approximately 33°C and the  $d(\Delta n)/dT$  of every LC increases sharply near its own isotropic temperature. The second example of an LMLC is an in-house (LLE) wave-plate mixture (60% 18523 and 40% 14627). This mixture has been used for LC optical devices at LLE and has proven to be convenient for conventional LC cell construction. The mixture does, however, show a higher birefringence change with temperature than does the NPLC LC360N and, for half-wave-plate construction at 1054 nm, would exhibit a slightly higher retardance change

Table 55.IV: Temperature dependence of refractive indices of NPLC at  $\lambda = 1054$  nm.

Temperature (°C)	$n_o$	$n_e$	$\Delta n$	$n_{av}$
20	1.5132±0.0002	1.6584±0.0002	0.1452±0.0004	1.5631±0.0002
30	1.5127±0.0002	1.6523±0.0002	0.1396±0.0004	1.5606±0.0002
40	1.5115±0.0001	1.6447±0.0002	0.1332±0.0003	1.5572±0.0001
50	1.5113±0.0003	1.6364±0.0002	0.1251±0.0005	1.5541±0.0003
60	1.5116±0.0002	1.6270±0.0001	0.1154±0.0003	1.5510±0.0002
70	1.5120±0.0001	1.6105±0.0004	0.0985±0.0005	1.5455±0.0002

with temperature. Finally, a newer LMLC, E200, shows a  $d(\Delta n)/dT$  at 20°C of  $(-)0.00009/\text{°C}$ , an order of magnitude smaller than our NPLC. A zero-order half-wave plate made of this LMLC would show only one-third the birefringence change of LC360N, but such a cell would require an external epoxy seal. Our NPLC shows promise for providing temperature-stable retardance in a thin, self-sealing cell.

### Wave-Plate Construction

This section describes the fabrication of NPLC wave plates using various substrate and spacer arrangements. All work with formic acid was performed in a Class 10 fume hood in a Class 1000 clean room. All cell construction, excluding degassing, was performed in a Class 10 laminar flow hood in a Class 1000 clean room.

For the double-substrate wave plates, our target retardance using an 18-μm-thick path length was 2614 nm. This provided a second-order retardance of 506 nm, i.e., a second-order half-wave plate at 1054 nm.

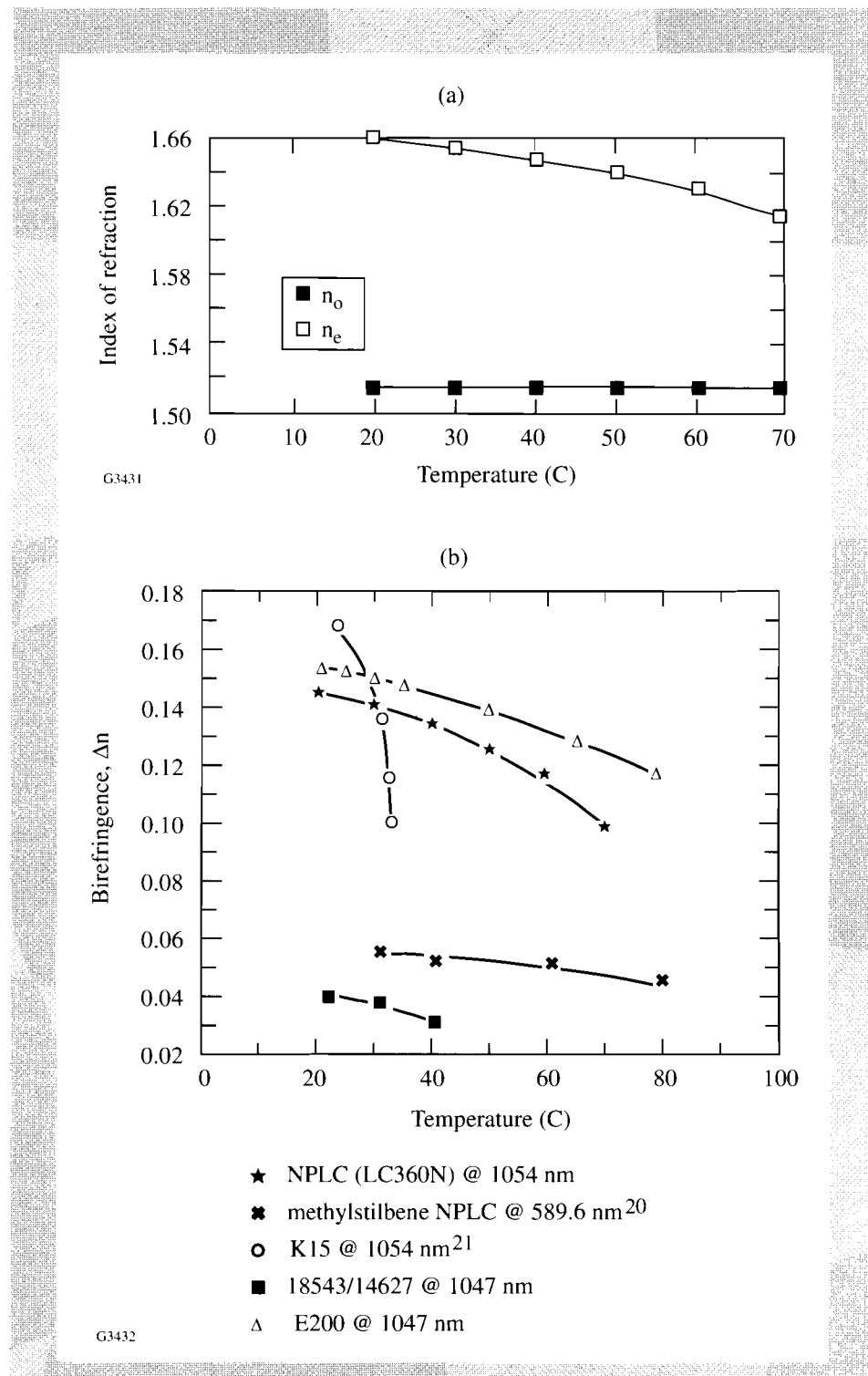


Fig. 55.29

Temperature dependence of refractive index for NPLC. (a)  $n_e$  and  $n_o$  between  $T = 20^\circ\text{C}$  and  $T = 70^\circ\text{C}$ . (b)  $\Delta n$  between  $T = 20^\circ\text{C}$  and  $T = 70^\circ\text{C}$ , compared to literature and measured data for several other LC compounds.

Table 55.V: Comparison of temperature dependence of birefringence of LC360N with other LC materials.

Material	LC360N	methylstilbene PLC	K15	60%18523 + 40% 14627	E200
Form	NPLC	NPLC	LMLC	LMLC	LMLC
$T_i$	88°C	~100°C	33°C	~50°C	88.5 °C
$\lambda$	1054 nm	589.6 nm	1054 nm	1047 nm	1047 nm
$\Delta n$ at 20°C	0.1452	0.057	0.168	0.042	0.152
$d(\Delta n)/dT$ at 20°C (1/°C)	$-2.755 \times 10^{-4}$	$-2.970 \times 10^{-5}$	$\sim -4.18 \times 10^{-3}$	$-3.35 \times 10^{-4}$	$-9.492 \times 10^{-5}$
$d(t\Delta n)/dT$ per $\mu\text{m}$ at 20°C (nm/°C/ $\mu\text{m}$ )	-0.2755	-0.0297	~-4.18	-0.335	-0.0942
$d(t\Delta n)/dT$ for $t = 527 \text{ nm}$ and 20°C (nm/°C/ $\mu\text{m}$ )	-0.1452	---	-2.202	-0.1766	-0.0496
Reference	---	20	21, 22	3, 22	22

### 1. Double-Substrate, Fiber-Spacer Homogeneous Distribution

The thickness of the NPLC layer was fixed using commercially available glass fiber spacers<sup>23</sup> mixed into the polymer. The fiber-spacer diameters were  $18 \pm 0.3 \mu\text{m}$  and lengths varied from 20 to 100  $\mu\text{m}$ . The fiber spacers were added to the polymer for a calculated yield of approximately 150 spacers in the completed cell (0.8 mg of fibers to 3.2 g of polymer). Homogeneous distribution of the fibers was achieved by heating the mixture to 100°C and stirring mechanically for 15 min. A small amount of the mixture was removed with a stirring rod and smeared onto a bare microscope slide. This smear was checked under a light microscope for homogeneous distribution (i.e., no clumping) of the fibers. Stirring introduced bubbles into the mixture, so it was degassed at 100°C and <1 Torr until bubbles were no longer visible (about 1 h for the given mass of polymer). The vacuum was applied gradually, 250 Torr every 15 min, to prevent excessive foaming of the NPLC.

The wave-plate substrates were two 50-mm-diam, 7-mm-thick borosilicate glass (BK7) discs polished to a surface flatness of better than  $\lambda/10 \text{ P-V}$  at 633 nm. Both were coated with a nylon 6/6 alignment layer using the procedure described under "3. Birefringence Measurement . . .". One substrate was heated to 100°C.

The polymer was separately heated to 100°C and scooped onto the substrate using a metal microspatula. The other substrate was kept at room temperature so that it could be lowered by hand onto the polymer. The rub directions of the substrates were antiparallel. The constructed cell was degassed at 100°C and <1 Torr for 24 h to remove trapped air bubbles. The cell was placed on a 5-mm-thick silica square, loaded onto a hotplate, covered with a Pyrex glass dish, held at 88°C for 24 h, and then cooled from 88°C to 20°C at 1°C/h. This was the same annealing protocol used for the birefringence measurement cell.

The completed cell had approximately 75 fibers distributed over the full aperture. There was little distortion of the NPLC alignment around these fibers as shown by viewing at 100X magnification between crossed polarizers [see Fig. 55.30(a)]. Annealing removed all evidence of fluid flow around the spacers.

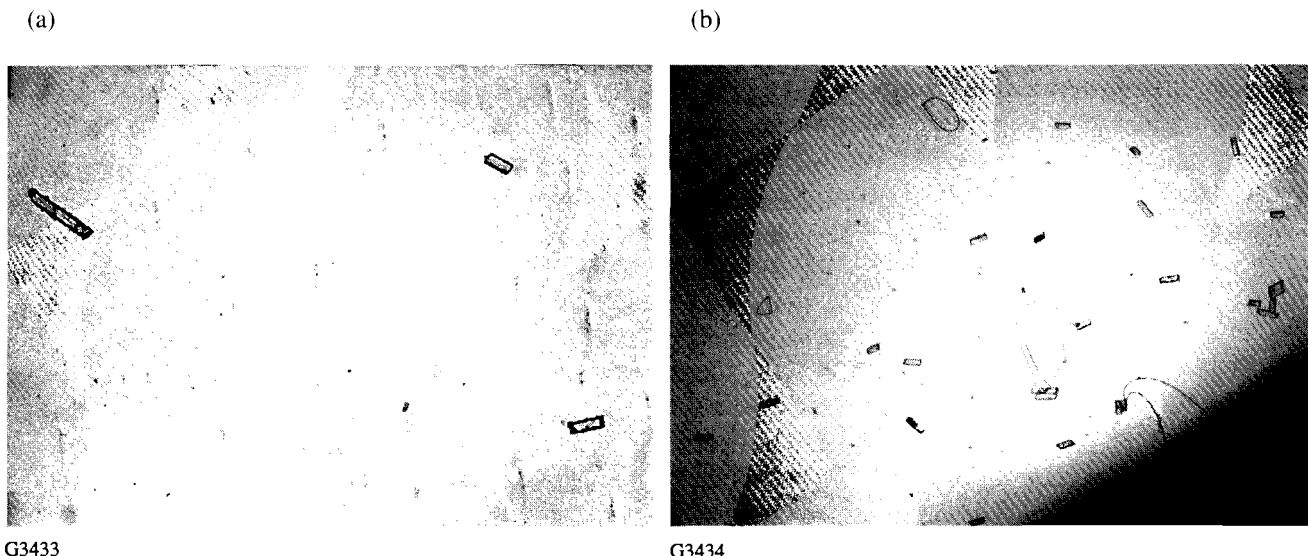


Fig. 55.30

Glass fiber spacers (18- $\mu\text{m}$  diam) in double-substrate wave plates. (a) Photograph at 100X magnification between crossed polarizers shows three fibers in a 0.8-mm<sup>2</sup> area in the double-substrate wave plate with homogeneous fiber distribution. There are no apparent disclinations. (b) Photograph at 50X magnification between crossed polarizers shows fibers in a 3-mm<sup>2</sup> area in double-substrate wave plate with fiber-spacer annulus. These fibers and the disclinations surrounding them are outside the clear aperture of the wave plate. Other features in both photomicrographs may be attributed to dirt or buffing marks.

## 2. Double-Substrate, Fiber-Spacer Annulus

An alternative technique was employed to keep the fiber spacers out of the wave plate's clear aperture where they might otherwise provide sites for laser damage or contribute to gradients in the transmitted optical wavefront. The fibers were applied in an annulus after the alignment layer had been applied and buffed. For 50-mm-diam BK7 substrates, a 32-mm-diam glass mask was placed over the clear aperture. The fibers were applied by dipping a cotton swab into the fibers, tapping them off above the substrate, and removing the mask; then the NPLC was applied by scooping it at 100°C onto the clear aperture of the substrate also held

at 100°C. As described in the preceding subsection, the procedure then continued with construction of the double-substrate cell. Both parallel and antiparallel construction were tested. Retardance values of the parallel and antiparallel cells were comparable, but total tilt angle varied [see “2. Wave-Plate Evaluation” in the next section].

The density of fibers in the annular region was high. Figure 55.30(b) (photograph taken at 50X magnification between crossed polarizers) shows a density of approximately 15 fibers per mm<sup>2</sup>. This contributed to the formation of lines of disclination, but this effect was confined to the annulus outside of the clear aperture and did not affect transmitted-wavefront quality or measured retardance.

### 3. Single Substrate

In addition to the methods described above for sandwich-type NPLC wave plates, we developed a method for producing single-substrate wave plates. Since a large proportion of the cost of any high-quality LC device is attributed to the substrates, a single-substrate wave plate essentially halves the expense of the device. A single substrate was prepared with an alignment layer as described previously. The single substrates used here were 12 mm thick.

The first procedure tested was spin-coating a solution of the NPLC in chloroform solvent (5% w/w) onto the buffed substrate. Solvent alone was dripped by syringe onto the substrate and allowed to sit for 30 s. The substrate was then spun at 1800 rpm while dripping solvent (1 ml) onto the substrate for a total spin of 60 s. Then the 5% solution was dripped by syringe onto the substrate, allowed to sit for 60 s, spun at room temperature at 1800 rpm again dripping 1 ml of the solution for the initial part of the spin, for a total spin of 120 s. The single substrate was annealed under the same protocol as the double-substrate cells. Viewing between crossed polarizers showed alignment and visual transmission/extinction contrast; however, retardance measurements by laser ratiometer were within the system noise levels, suggesting that the NPLC layer was too thin to measure. Microscopic examination showed beading of the NPLC along the rub direction. Higher concentrations did not spin on uniformly.

A second method was attempted that involved dripping the NPLC/chloroform solution onto the buffed substrate and allowing the solvent to evaporate, leaving behind the NPLC layer. Low concentrations (<7%) evaporated so rapidly that the NPLC was deposited in uneven patches. Evaporation of higher-concentration solutions left a polymer-layer barrier at the air/solution interface that precluded further evaporation.

Consequently, the NPLC had to be applied directly to the buffed substrate in the following way: The substrate was placed on a silica square and heated to 100°C. NPLC at 100°C was scooped along one edge to form a crescent. A stainless steel rod of wound stainless steel wire,<sup>24</sup> designed to give a thickness of 6 µm, was used to stroke the NPLC across the substrate either parallel or perpendicular to the buff direction for a given trial. To prevent sliding of the substrate, glass tacks were epoxied at one corner of the silica square. The cell was transferred to a plain silica square, held in an oven at 88°C for 1 h, then allowed

to cool to room temperature (average rate of cooling was  $\sim 20^\circ\text{C}/\text{h}$ ). Longer heating (2 h) with slower annealing ( $3^\circ\text{C}/\text{h}$ ) showed no improvement in uniformity or alignment. There was no significant difference in uniformity or alignment between single-substrate cells made with flat ( $PV < \lambda/10$ ) and nonflat ( $PV \sim 5\lambda$ ) substrates, nor for stroking of NPLC with the steel rod perpendicular versus parallel to the rub direction. Neither the bulk NPLC nor that on the substrate was degassed since previous experiments with degassing showed no improvement in appearance.

All trials showed a residual outline of the original crescent-shaped NPLC application region. Partial removal of this nonuniformity was achieved by using a combination of application techniques. A buffed substrate sitting on a silica square with glass tacks at one corner was heated to  $100^\circ\text{C}$ . The NPLC, also at  $100^\circ\text{C}$ , was scooped onto the center of the substrate. A small brush was used to spread the NPLC smoothly over the surface. Brush strokes were either parallel or perpendicular to the buff direction for a given trial. As described above, the warmed rod was drawn across the surface to promote uniform thickness. This cell was held at  $110^\circ\text{C}$  for 15 min. The hot cell was then spun at 4000 rpm for 30 s to evenly distribute the NPLC over the substrate and to remove any residual brush or rod lines. (This process step dictated the use of thick, single substrates. Their large heat capacity ensured that the NPLC was warm enough to flow during the entire spin.) This cell was held in an oven as before at  $88^\circ\text{C}$  for 1 h, then allowed to cool to room temperature. The brush did introduce some air bubbles, but they disappeared during the 1 h of heating.

### Wave-Plate Evaluation

The optical quality of a wave plate depends on undistorted wavefront transmission over the clear aperture and on accuracy and uniformity of retardance. Constructed wave plates were first viewed between crossed polarizers for uniformity of transmission and extinction.

Table 55.VI gives transmitted-wavefront distortion with and without the NPLC; retardance; tilt angle at center and over the clear apertures (75% of the hard apertures); and thickness calculated from total retardance and tilt angle<sup>25</sup> for all three types of wave plates.

#### 1. Transmitted Wavefront

Transmitted wavefront was measured using a Fizeau interferometer<sup>26</sup> at  $\lambda = 633 \text{ nm}$ . To establish a transmitted-wavefront reference, the substrates ultimately used in the double-substrate configuration were first assembled with 5- $\mu\text{m}$  Mylar<sup>27</sup> spacers and index-matching fluid<sup>17</sup> ( $n_D = 1.516$ ). Three external glass tacks, epoxied across the sides of the substrates, maintained the cell structure for interferometry. The transmitted-wavefront quality of this “mock” cell was used as a standard of comparison for the double-substrate cell subsequently assembled. The reference for the single substrate was the substrate itself.

Transmitted-wavefront distortion for all three types of cells varied from 2 to 4 times that of the blank cell. One double-substrate cell, stored vertically for one month, showed transmitted-wavefront improvement of about  $0.1 \lambda$ . Such

Table 55.VI: Results of wave-plate evaluations.

Wave Plate	Double-Substrate, Homogeneous Fiber Distribution	Double-Substrate, Fiber Annulus	Single Substrate
@ 633 nm			
Transmitted wavefront distortion, no NPLC (reference)	$0.073 \pm 0.015 \lambda$	$0.073 \pm 0.015 \lambda$	$0.781 \pm 0.043 \lambda$
Transmitted wavefront distortion, NPLC	$0.404 \pm 0.050 \lambda$	$0.382 \pm 0.048 \lambda$	$1.544 \pm 0.237 \lambda$
@ 1054 nm			
Retardance design goal	$506 \pm 40 \text{ nm}$ (second order)	$506 \pm 40 \text{ nm}$ (second order)	----
Measured average retardance	$496.9 \pm 11.3 \text{ nm}$ (second order)	$510 \pm 28 \text{ nm}$ (second order)	$416 \pm 42 \text{ nm}$ (first order)
Tilt angle (single spot)	$2.36 \pm 0.31^\circ$	$0.37 \pm 0.15^\circ$	$0.5 \pm 0.5^\circ$
Average tilt angle (nine spots)	$1.31 \pm 0.95^\circ$	$0.11 \pm 0.09^\circ$	$0.6 \pm 0.3^\circ$
Thickness based on retardance and tilt angle	$17.95 \pm 0.08 \mu\text{m}$	$18.03 \pm 0.19 \mu\text{m}$	$10.13 \pm 0.28 \mu\text{m}$

improvement might be desirable but points out the susceptibility of an NPLC like LC360N to flow under the influence of gravity when the glass transition temperature is too near room temperature.

## 2. Retardance

a. Value and variation. Retardance was measured using a laser ratiometer with a Soleil-Babinet compensator<sup>28</sup> between crossed Glan-Thompson calcite polarizers. The approximate laser-beam diameter at the cell location was 2 mm. The retardance order was established by the fiber-spacer diameter. Nine spots were measured and averaged. Single-spot retardance was measured five times at the center to establish reproducibility. Variation was no more than  $\pm 5 \text{ nm}$  for all types of wave plates.

Both types of double-substrate wave plates showed excellent agreement of expected and average measured retardance values. Due to the near-room-temperature glass transition of the NPLC, any manipulation of the cell by hand contributed to some degradation of retardance uniformity. Retardance uniformity was most dependent on fiber-spacer distribution. In the homogeneous distribution

type, as few as 75 spacers over the aperture provided excellent gap uniformity [see Fig. 55.31(a)]. In the fiber annulus distribution type, the density of fibers was more difficult to control. Regions of excessive fiber deposition led to more severe gap wedges [see Fig. 55.31(b)]. More uniform and reproducible gaps were obtained by swabbing fibers directly onto the exposed substrate around the mask than by tapping from a swab. However, direct swabbing scratched the nylon alignment layer, creating regions of scattering that sometimes extended into the clear aperture.

The single-substrate wave plate showed fairly good uniformity over most of the clear aperture. Variations in thickness, i.e., wedge, were commonly caused by unevenness of stroking with the hand-coater rod [see Fig. 55.31(c)].

For use in a laser system, a retardance deviation of no more than  $\pm 10\%$  of the calculated value is desirable.<sup>29</sup> All three types of wave plates showed this accuracy when averaged over the aperture. However, this specification presumes uniformity across the clear aperture. Only the double-substrate wave plate, having fiber spacers in homogeneous distribution, showed sufficient uniformity for use in a high-peak-power laser system. Improved uniformity of other wave-plate types may be expected with refinements in the application of (a) fibers, in the case of the annular-distribution double-substrate wave plate, or (b) NPLC, in the case of the single-substrate wave plate.

**b. Tilt angle.** Tilt angle is the angle that the side chains of the NPLC make with respect to the substrate surface. The tilt angle was measured at the center of the cell for reproducibility tests and at nine spots for uniformity tests using a phase-retardation method<sup>25</sup> in which the cell is rotated around an axis perpendicular to the incident beam in a laser ratiometer.

Because the tilt-angle measurement is an average through the cell, parallel construction of the double-substrate cells yielded tilt-angle measurements of almost zero, whereas antiparallel construction led to tilt-angle measurements of  $2^\circ$ – $3^\circ$ . This is consistent with the induced tilt angle being the same at both inner surfaces.<sup>30</sup> The tilt of the side chains at the first surface induces a slight retardance on the incident beam. In parallel construction, this beam then encounters side chains at the second surface that are tilted in the opposite direction compensating for the retardance. As the cell is rotated around an axis perpendicular to the incident-beam, a minimum in transmission indicates a matching of the incident-beam polarization with the side-chain tilt. For the parallel cell, this minimum occurs at normal incidence, where retardance of one surface just compensates the other. In antiparallel construction, no such compensation takes place, in which case a minimum in transmission occurs at an off-normal angle if side-chain tilt exists. Table 55.VI reports the tilt angles for (1) a double-substrate wave plate with homogeneous distribution of fibers and antiparallel construction and (2) a double-substrate wave plate with fibers in an annular distribution and parallel construction. The tilt angle of the NPLC on the single substrate was negligible.

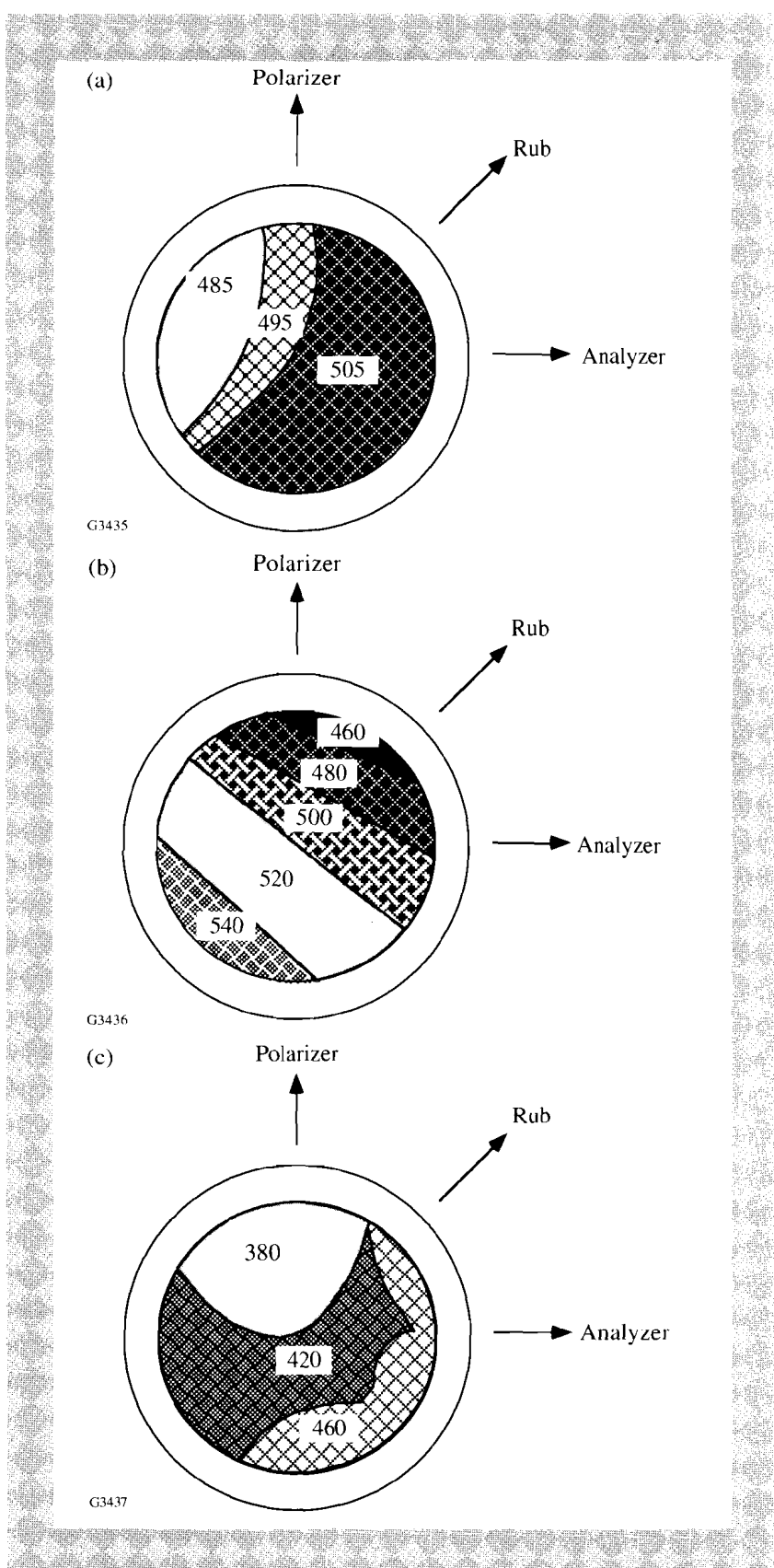


Fig. 55.31  
 Wave-plate retardance contour maps. Retardance is measured using a Soleil-Babinet compensator.  
 (a) Double-substrate homogeneous fibers—values shown represent  $\pm 5$  nm of second-order retardance within the indicated region; (b) double-substrate fiber annulus—values shown represent  $\pm 10$  nm of second-order retardance within the indicated region; (c) single substrate—values shown represent  $\pm 20$  nm of first-order retardance within the indicated region.

c. Thickness. Since there was a range in diameters of fiber spacers used for the double-substrate cells, total retardance was used to calculate the thickness of the NPLC, and the fiber thickness was used to establish the order of retardance. The retardance used for thickness calculations had to be corrected for that retardance due to tilt angle.<sup>25</sup> The thicknesses shown in Table 55.VI are based on these corrected total-retardance values. Even without the correction, measured thickness values of the NPLC layer were well within the range established by the fiber-spacer diameter. This result implies that the fibers maintained the cell gap without trapping any NPLC between the fiber and the substrate.

### Laser-Damage Resistance

The NPLC wave plates constructed and evaluated above provide numerous advantages over both traditional crystalline solids and low-molecular-weight liquid crystals for typical optical uses. However, the particular NPLC used for this study provided yet another advantageous property—high laser-damage resistance.

The laser-damage resistance of the LC360N was measured at 1054 nm by a technique described in greater detail elsewhere.<sup>2</sup> The NPLC was dissolved in toluene (at 2% w/w solids content) and sprayed by airbrush onto the small face of a 30-60-90 BK7 prism, the geometry of which prevents back reflection and subsequent interference effects. Both 1-on-1 and *N*-on-1 tests were made. In 1-on-1 tests, a single laser pulse is incident on a previously nonirradiated site. The energy within the pulse is gradually increased at each new location until damage is seen. In *N*-on-1 testing, laser pulses of increasing energy are incident on the same site at 5-s intervals until damage is seen. The laser used was a Nd:glass, mode-locked, feedback-controlled, Q-switched oscillator, whose 1054-nm pulses could be frequency-tripled to 351 nm using KDP. Pulses were  $1\pm0.1$  ns in duration in the IR (3 J/pulse). Damage was diagnosed as the appearance, within the 3-mm-diam irradiation spot size, of a bubble that scattered light. Under Nomarski microscopic inspection [Fig. 55.32(a)], the NPLC exhibited apparent multiple-clustered pitting.

The original brown sample of LC360N was contaminated with traces of a polymerization catalyst believed to be colloidal metallic platinum with considerable potential for causing laser damage. After purification to 1 ppm Pt by column chromatography (purification carried out by Wacker Chemie), the clear, colorless polymer showed a much-improved laser-damage resistance, and the laser-damage sites showed far less severe pitting [see Fig. 55.32(b)].

The laser-damage test data are reported in Table 55.VII. The films used in damage testing were 2.5 times thicker than the NPLC in the second-order wave plates and 13 times thicker than an NPLC layer required for a zero-order wave plate. Since laser-damage resistance can be expected to improve for thinner layers, damage thresholds for NPLC wave plates in a working system would likely be even higher than those reported here. The laser-damage measurements of a nylon alignment layer,<sup>3</sup> buffed under both hard and light conditions, show resistance of 5 to 10 J/cm<sup>2</sup> (Table 55.VII). Damage-resistance levels of several J/cm<sup>2</sup> are compatible for use in many high-peak-power laser applications. The components of an NPLC wave plate with a nylon alignment layer meet this specification.

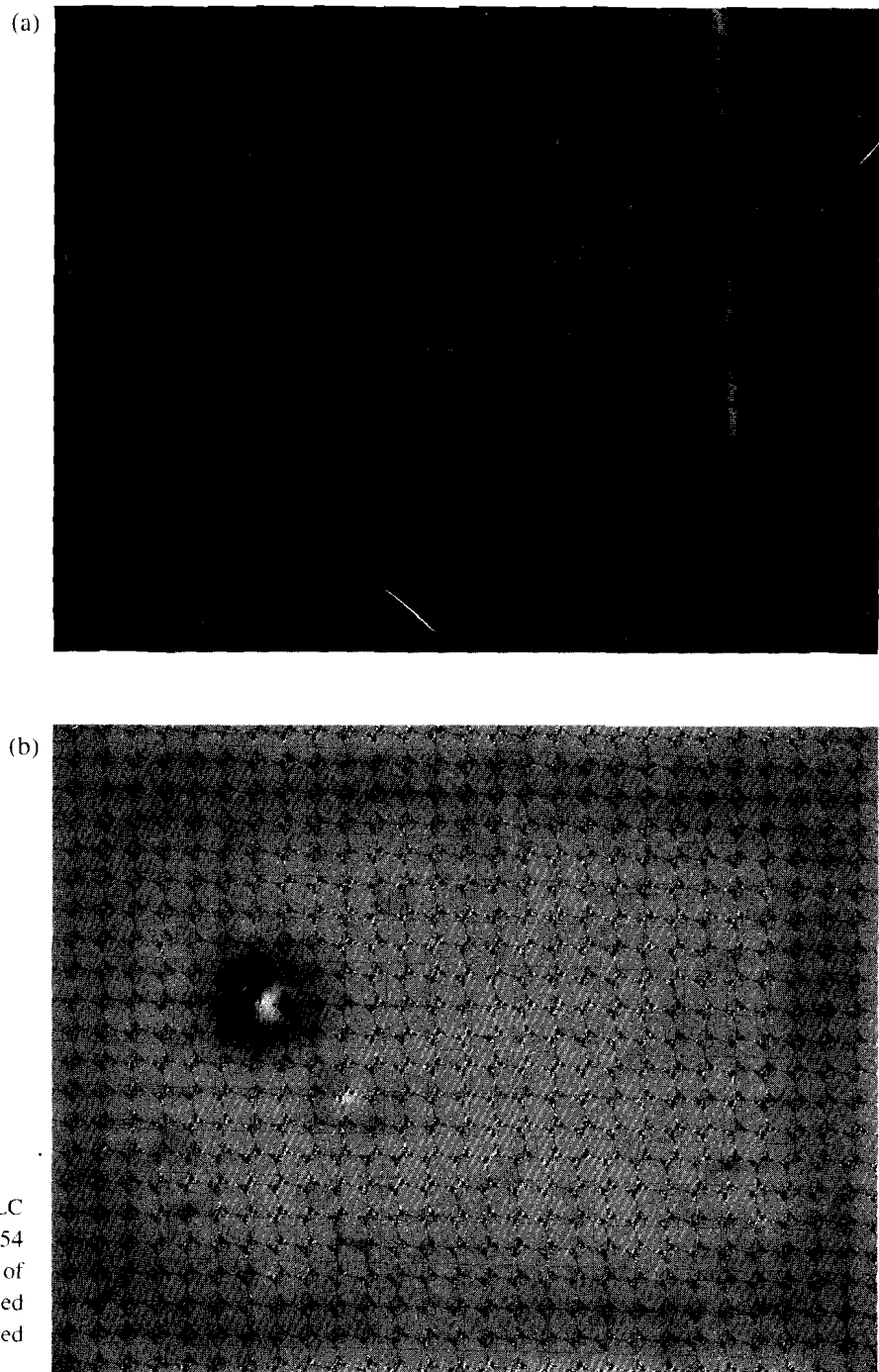


Fig. 55.32

Nomarski photomicrographs (100X) of NPLC after irradiation with a 1-ns laser pulse at 1054 nm. (a) Extensive pitting in a 16- $\mu\text{m}$  layer of unpurified material (39 ppm Pt). (b) Reduced incidence of damage in a 45- $\mu\text{m}$  layer of purified material (1.0 ppm Pt).

G3438

### Summary

We have developed techniques for using a nematic polymer liquid crystal in the construction of a wave plate. These techniques include measurement of the birefringence of the highly viscous NPLC and alignment by thermal annealing against a buffed nylon 6/6 aligning layer. We were able to construct three types of wave plates—double substrate with fiber spacers distributed homogeneously;

Table 55.VII: Laser-damage resistance of nematic polymer LC360N and nylon 6/6.

Pattern	Material	Damage Threshold (J/cm <sup>2</sup> ) @ 1 ns, 1054 nm
1-on-1	16-μm film, unpurified	1.0±0.1
N-on-1		0.8±0.1
1-on-1	45-μm film, purified to 1 ppm Pt	1.4±0.2
N-on-1		3.2±0.3
1-on-1	nylon 6/6, light buff	5.5±0.9
	nylon 6/6, hard buff	6.57±0.07
N-on-1	nylon 6/6, light buff	9.5±0.4
	nylon 6/6, hard buff	5.9±0.8

double substrate with fiber spacers distributed in an annulus; and single substrate. The viscosity/temperature behavior of the NPLC allowed alignment at higher temperatures but configuration stability at lower (room) temperature. The NPLC acted as its own adhesive to seal the confining substrates together. The high laser-damage resistance of the NPLC indicates that it and similar materials will prove useful for high-peak-power laser applications.

The wave plates showed promising uniformity and transmitted-wavefront quality as well as the capability of meeting specific retardance requirements at a cost determined mainly by the glass substrates. Further improvements in device stability could be obtained by using an NPLC with a higher glass-transition temperature (>40°C to ensure a “locked-in” configuration at room temperature, to allow greater ease of handling, and to eliminate long-term flow under the influence of gravity). If the NPLC had a positive dielectric anisotropy ( $\Delta\epsilon$ ), molecular alignment would be facilitated by allowing annealing in the presence of an electric field.

#### ACKNOWLEDGMENT

The authors wish to thank Mark J. Guardalben for providing photographs of damaged NPLC; Kenneth L. Marshall for discussions regarding NPLC alignment and manuscript preparation; and Semyon Papernov for discussion of damage-testing methodology. This work was supported by the U.S. Department of Energy Office of Inertial Confinement Fusion under Cooperative Agreement No. DE-FC03-92SF19460, the University of Rochester, and the New York State Energy Research and Development Authority. The support of DOE does not constitute an endorsement by DOE of the views expressed in this article.

## REFERENCES

1. S. D. Jacobs, K. A. Cerqua, K. L. Marshall, A. Schmid, M. J. Guardalben, and K. J. Skerrett, *J. Opt. Soc. Am. B* **5**, 1962 (1988).
2. M. Guardalben, A. Bevin, K. Marshall, A. Schmid, and F. Kreuzer, in *Laser Induced Damage in Optical Materials: 1988*, Natl. Inst. Stand. Technol. (U.S.), Spec. Publ. 775 (U.S. Government Printing Office, Washington, DC, 1989), pp. 462–469.
3. A. L. Rigatti, D. M. Dudek, R. G. Carnes, L. D. Lund, K. L. Marshall, S. Papernov, A. W. Schmid, D. J. Smith, and S. D. Jacobs, presented at CLEO '93, Baltimore, MD, 2–7 May 1993.
4. S. D. Jacobs, K. L. Marshall, and K. A. Cerqua, U. S. Patent No. 5,054,888 (8 October 1991).
5. Nylon 6/6 (polyhexamethylene adipamide) pellets, Polysciences, Inc., Warrington, PA 18976, Cat. #6557.
6. LC360N, nematic polymer liquid crystal provided through F. Kreuzer in association with Wacker Chemie, Munich.
7. Brookfield Digital Viscometer Model DV-II equipped with Helipath Stand. The T-bar-type spindle used was T-F, #96; the disc spindle was RV6.
8. Lauda Refrigerating Circulator, Model RMS6, Brinkman Instruments, Inc., Cantiague Road, Westbury, NY 11590.
9. M. C. Muir and R. S. Porter, *Mol. Cryst. Liq. Cryst.* **169**, 83 (1989).
10. G. Marrucci, in *Liquid Crystallinity in Polymers: Principles and Fundamental Properties*, edited by A. Ciferri (VCH Publishers, New York, 1991), Chap. 11.
11. Bellingham and Stanley Model 60/HR Abbe Refractometer, Bellingham and Stanley Limited, Longfield Road, North Farm Industrial Estate, Tunbridge Wells, Kent TN2 3EY, England.
12. Bellingham and Stanley Calibration Tables for Abbe Refractometer Model 60/HR.
13. J. Kelly Houghton (unpublished research results).
14. Dataplate Digital Hot Plate/Stirrer, PMC Industries, Inc., 6335 Ferris Square, San Diego, CA 92121-3208.
15. TexTech Industries, Main Street, North Monmouth, ME 04265.
16. Digimatic Indicator IDC Series 543, Mitutoyo Corporation, 31-19, Shiba 5-chome, Minato-ku, Tokyo 108, Japan.
17. R. P. Cargille Laboratories, Inc., Cedar Grove, NJ.
18. Find-R-Scope, FJW#84499 (maximum range of wavelength sensitivity is 1.2 μm), FJW Optical Systems, Inc., 629 South Vermont Street, Palatine, IL 60067.

19. J. M. Bennett and A. T. Glassman, in *CRC Handbook of Laser Science and Technology, Section 1.4: Optical Materials*, edited by M. J. Weber (CRC Press, Boca Raton, FL, 1986), Vol. IV, Part 2: Properties, p. 227.
20. N. A. Vaz *et al.*, Mol. Cryst. Liq. Cryst. **198**, 305 (1991).
21. K. C. Chu, C. K. Chen, and Y. R. Shen, Mol. Cryst. Liq. Cryst. **59**, 97 (1980).
22. Nematic LMLC's, EM Industries, Inc., Advanced Chemical Division, 5 Skyline Drive, Hawthorne, NY 10532.
23. Ultra Precision Glass Fibers, EM Industries, Inc., Advanced Chemical Division, 5 Skyline Drive, Hawthorne, NY 10532, 18- $\mu\text{m}$  fiber spacers - Cat. #111357.
24. K Hand Coater, RK Print-Coat Instruments Ltd., South View Laboratories, Litlington, Royston, Herts SG8 0QZ.
25. H. L. Ong, J. Appl. Phys. **71**, 140 (1992).
26. Zygo Mark IVxp, Zygo Corporation, Laurel Brook Road, P.O. Box 448, Middlefield, CT 06455-0448.
27. Mylar (polyethylene terephthalate), DuPont Company, Electronics Department, MYLAR Customer Service, Barley Mill Plaza, P.O. Box 80019, Wilmington, DE 19880-0019.
28. Soleil-Babinet Compensator Model 8-400, Special Optics, 101 E. Main Street, P.O. Box 163, Little Falls, NY 07424.
29. C. Cotton (private communication).
30. G. Baur, V. Wittwer, and D. W. Berreman, Phys. Lett. **56A**, 142 (1976).